Supplementary Material

1 SIMULATIONS

1.1 DFT-MD

The density-functional molecular dynamics (DFT-MD) simulations were performed using the package VASP Kresse and Hafner (1993, 1994); Kresse and Furthmüller (1996a,b). The electronic density was represented by a plane wave expansion with cut-off energy of $E_{cut} = 1000$ eV. We used the Mermin formulation of DFT to optimize the Helmholtz free energy at a given temperature Mermin (1965). The electron-ion interaction was modeled using the projector augmented wave (PAW) approach Blöchl (1994); Kresse and Joubert (1999). The exchange correlation potential was used in a generalized gradient approximation via Perdew-Burke-Ernzerhof parametrisation (GGA-PBE) Perdew et al. (1996, 1997). The simulation generally sampled the Brillouin zone of the supercell at the Γ-point only. The electronic bands were populated using a Fermi distribution at the chosen temperature. A significant increase in the number of available bands, $N_{bands} = 1300$, was required for the 64 electrons to capture the tail of the Fermi distribution at $T_e = 10$ eV.

The supercell contained 64 protons whose movements, according to Newton mechanics, were calculated using the proton-proton potentials and the electron-ion Hellman-Feynman forces derived from the electron densities of DFT in Born-Oppenheimer approximation. The time step was $\Delta t = 0.2$ fs and the DFT-MD runs feature approximately 3600 steps. For two-temperature runs at given electron and ion temperatures, the ion temperature was controlled by a Nosé-Hoover thermostat Nosé (1984). Such two-temperature DFT-MD simulations were previously used to model the energy relaxation in similar pump-probe experiments at FLASH Zastrau et al. (2014).

1.2 HNC

Our version of an HNC code takes hydrogen atoms and protons explicitly into account as two different species Springer et al. (1973); Wünsch et al. (2008, 2009). The free electrons are not modeled explicitly, but screen the proton-proton and proton-atom interaction via linear response. Consequently, the proton-proton interaction is given by a Debye potential featuring a screening length for arbitrary degeneracy. The atom-atom potential is of the exp-6 functional form as given in Ref. Juranek and Redmer (2000). The proton-atom interaction is described by way of an optical potential Redmer (1997)

$$\begin{aligned} V_{pH}^{opt}(r) &= e^2 \left[\left(\frac{1}{r} + \frac{1}{a_B} \right) \exp(-2r/a_B) \right. \\ &\quad \left. + \frac{\alpha_D}{2} \left(\frac{1+\kappa r}{r^2 + r_0^2} \right)^2 \exp(-2\kappa r) \right] . \end{aligned} \tag{S1}$$

Here, $\alpha_D = 4.5\,\mathrm{a}_B^3$ is the dipole polarisability, and $r_0 = 1.456\,\mathrm{a}_B$ the cut-off parameter for a hydrogen atom. For small proton and atom temperatures, where we expected strong coupling, we supplemented and validated the HNC calculations with classical Monte Carlo (MC) simulations featuring the same potentials as the HNC calculations. Overall, static structure calculations where performed for the matrix of all combinations of $T_i = 1 \ldots 10$ eV and $T_e = 1 \ldots 10$ eV in 1 eV steps.

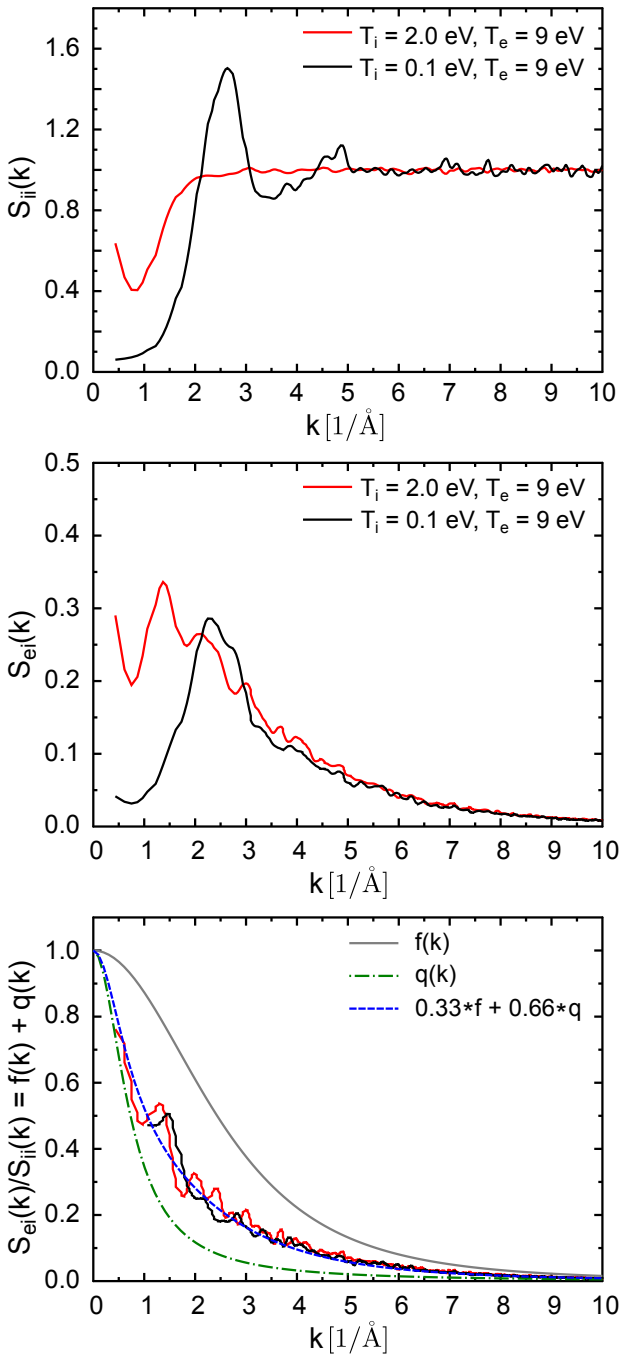

Figure S1. Static partial structure factor of two-temperature hydrogen from DFT-MD simulations at $\rho = 0.07$ g/cm^3, $T_e = 10$ eV. (*top*) ion-ion structure factor, (*middle*) electron-ion structure factor, (*bottom*) generalized screening cloud and fit of average charge.

The amount of ionization may be inferred from computation of the ion-ion and ion-electron static structure factors, see Fig. S1. For both conditions given in Fig. S1, the ion structure does not show any signs of molecules, instead it is dominated by Coulomb correlations.

1.3 3D PIC

In order to model the intense laser-plasma interaction and fast electron dynamics we have performed 3D PIC simulations of the experimental conditions with the code OSIRIS Fonseca et al. (2002, 2008). The laser pulse is modeled using a Gaussian-shaped temporal and spatial profile with FWHM duration $\tau_{laser} = 70$ fs and spot size $W_{laser} = 6$ μm. The laser wavelength is 0.4μm and peak intensity is 5×10^{17} W/cm^2, corresponding to a normalized vector potential $a_0 = 0.24$. The hydrogen jet has a 5 μm diameter with constant plasma density of 3×10^{22} cm^{-3}, as measured experimentally. The 3D simulation box size is $(16\mu\text{m})^3$ and is resolved with 768^3 cells, 8 particles/cell per species (electrons and protons), and a time step of 0.04 fs. The simulations were run on the supercomputer Mira at the Argonne National Laboratory in 65,536 computational cores. The simulation results show that during the laser-plasma interaction, fast electrons are produced at the surface, mostly via $J \times B$ heating Kruer (1988), with a slope temperature of 14.3 keV, which is consistent with ponderomotive scaling estimates Wilks (1993).

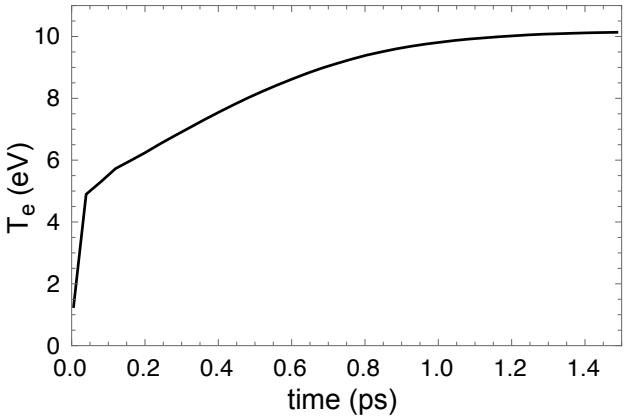

Figure S2. Evolution of the volume averaged plasma electron temperature (T_e) from 3D PIC simulations of the laser-plasma interaction. The peak laser intensity reaches the target at t = 0 and heats the surface to $T_e > 100$ eV. Fast electrons produced by the laser then recirculate through the target heating the background plasma. Fast and background populations equilibrate around 1 ps to $T_e \sim 10$ eV.

Around the end of the laser-plasma interaction, the jet surface hit by the laser reaches a temperature of $T_e \gtrsim 100$ eV, but the bulk of the target remains cold. Fast electrons then recirculate through the jet in t $<$ 100 fs and can heat the background electrons through a combination of collective and collisional processes. We observe that by t $\sim$ 1 ps, all fast electrons have thermalized with the background electrons and T_e becomes relatively uniform throughout the jet region modeled. Figure S2 shows the evolution of the background electron temperature averaged over the jet volume modeled, which closely corresponds to the experimental scattering volume. We can observe that electron equilibration is reached around 1 ps with $< Te > \sim 10eV$, consistent with the experimental data.

REFERENCES

Kresse G, Hafner J. Ab initio molecular dynamics for liquid metals. *Phys. Rev. B* **47** (1993) 558.

Kresse G, Hafner J. Ab initio molecular-dynamics simulation of the liquid-metal-amorphous-semiconductor transition in germanium. *Phys. Rev. B* **49** (1994) 14251.

Kresse G, Furthmüller J. Efficiency of ab-initio total energy calculations for metals and semiconductors using a plane-wave basis set. *Comp. Mat. Sci.* **6** (1996a) 15–50.

Kresse G, Furthmüller J. Efficient iterative schemes for ab initio total-energy calculations using a plane-wave basis set. *Phys. Rev. B* **54** (1996b) 11169.

Mermin ND. Thermal properties of the inhomogeneous electron gas. *Phys. Rev.* **137** (1965) A1441.

Blöchl PE. Projector augmented-wave method. *Phys. Rev. B* **50** (1994) 17953.

Kresse G, Joubert D. From ultrasoft pseudopotentials to the projector augmented-wave method. *Phys. Rev. B* **59** (1999) 1758.

Perdew JP, Burke K, Ernzerhof M. Generalized gradient approximation made simple. *Phys. Rev. Lett.* **77** (1996) 3865.

Perdew JP, Burke K, Ernzerhof M. *Phys. Rev. Lett.* **78** (1997).

Nosé S. A unified formulation of the constant temperature molecular dynamics methods. *The Journal of Chemical Physics* **81** (1984) 511–519. doi:10.1063/1.447334.

Zastrau U, Sperling P, Harmand M, Becker A, Bornath T, Bredow R, et al. Resolving ultrafast heating of dense cryogenic hydrogen. *Physical review letters* **112** (2014) 105002.

Springer J, Pokrant M, Stevens Jr F. Integral equation solutions for the classical electron gas. *J. Chem. Phys.* **58** (1973) 4863–4867.

Wünsch K, Hilse P, Schlanges M, Gericke DO. Structure of strongly coupled multicomponent plasmas. *Phys. Rev. E* **77** (2008) 056404.

Wünsch K, Vorberger J, Gericke DO. Ion structure in warm dense matter: Benchmarking solutions of hypernetted-chain equations by first-principle simulations. *Phys. Rev. E* **79** (2009) 010201.

Juranek H, Redmer R. Self-consistent fluid variational theory for pressure dissociation in dense hydrogen. *J. Chem. Phys.* **112** (2000) 3780–3786.

Redmer R. Physical properties of dense, low-temperature plasmas. *Phys. Rep.* **282** (1997) 35–157.

Fonseca RA, Silva LO, Tsung FS, Decyk VK, Lu W, Ren C, et al. Osiris: a three-dimensional, fully relativistic particle in cell code for modeling plasma based accelerators. *ICCS* (Springer) (2002), 342–351.

Fonseca R, Martins S, Silva L, Tonge J, Tsung F, Mori W. One-to-one direct modeling of experiments and astrophysical scenarios: pushing the envelope on kinetic plasma simulations. *Plasma Phys. Controlled Fusion* **50** (2008) 124034.

Kruer WL. *The physics of laser plasma interactions* (Addison-Wesley Pub. Co. Inc., Reading, MA) (1988).

Wilks SC. Simulations of ultraintense laser–plasma interactions. *Physics of Fluids B: Plasma Physics* **5** (1993) 2603–2608.